The electrochemical reduction of VO2+ in acidic solution at high overpotentials

Gattrell, M.; Qian, J.; Stewart, C.; Graham, P.; MacDougall, B.

Publisher's version / Version de l'éditeur:
https://doi.org/10.1016/j.electacta.2005.05.001
Electrochimica Acta, 51, 3, pp. 395-407, 2005

Available online at www.sciencedirect.com
SCIENCE DIRECT®
Electrochimica Acta 51 (2005) 395–407
ELECTROCHIMICA Acta
www.elsevier.com/locate/electacta

The electrochemical reduction of VO_2^+ in acidic solution at high overpotentials

M. Gattrell*, J. Qian, C. Stewart, P. Graham, B. MacDougall

National Research Council of Canada, Institute for Chemical Process and Environmental Technology, 1200 Montreal Road, Ottawa, Canada K1A 0R6

Received 5 March 2005; received in revised form 2 May 2005; accepted 2 May 2005
Available online 31 May 2005

Abstract

An investigation has been carried out to attempt to understand the unusually low apparent symmetry factor observed during the reduction of V(5) at higher overpotentials at carbon electrodes (typically <0.13, or >460 mV decade^{-1}). This reaction is of interest because it occurs in vanadium redox-flow batteries (VRBs) during discharge. Polarisation curves were measured using a rotating disk electrode (RDE). The reaction was not solution mass transport controlled, was pH independent (ca from 0 to 1), and the observed Tafel slope was unaffected by V(5) concentration over a range from 0.031 to 280 mM. Electrode double layer capacitance measurements were also carried out in sulphuric acid with and without vanadium. These tests showed that the presence of V(5) caused a suppression of the normal carbon surface quinone pseudocapacitance, as well as the appearance of two new pseudocapacitance peaks, one around 0.175–0.2 V and the other around 0.675–0.725 V versus SCE. The observed results do not appear consistent with a precipitated film causing diffusion limitations or causing IR drop. A model is developed to try to explain the data, which involves electron transfer through an adsorbed layer of vanadium.

Keywords: Vanadium; High Tafel slope; Adsorbed intermediates; Carbon electrodes; VRBs

1. Introduction

Redox-flow batteries show great promise for economical storage of electrical energy [1,2]. Redox-flow batteries are an electrochemical energy storage technology where the energy, rather than being stored at the electrodes like batteries, is stored by chemical changes to species dissolved in a working fluid. At the positive electrode a solution with a more anodic redox couple is circulated, while at the negative electrode a more cathodic redox couple is used. The two sides of the cell are typically separated with an ion exchange membrane to control mixing of the two solutions (a diagram of a vanadium-based system is shown in Fig. 1). The system power is determined by the rate of reaction of the redox species at each electrode and the total surface area of the electrodes. The concentration of the redox species and the volume of the reservoirs determine the amount of energy stored in the system. Because of this, the cost of a system will increase with the power output of the system based on the cost of the electrochemical cell, and the cost will increase with the energy storage capacity of the system based on the (typically lower) cost of the reservoirs and the working solutions. Thus, redox flow type batteries are particularly suited for longer-term energy storage. Finally, because the energy density is typically low (being limited by the solubility of the redox active compounds), the development of these systems has focused on stationary applications.

Such stationary storage of electricity can allow better matching of power generator outputs and fluctuating loads. Electricity storage can greatly increase the usefulness of non-continuous renewable power sources such as solar, wind, or tidal power [3]. If electricity storage could be made sufficiently inexpensive, it could also change the way in which electrical energy is generated, distributed, marketed, and used [4].

* Corresponding author. Tel.: +1 6139903819; fax: +1 6139912384.
E-mail address: michael.gattrell@nrc-cnrc.gc.ca (M. Gattrell).

0013-4686/$ – see front matter © 2005 Elsevier Ltd. All rights reserved.
doi:10.1016/j.electacta.2005.05.001

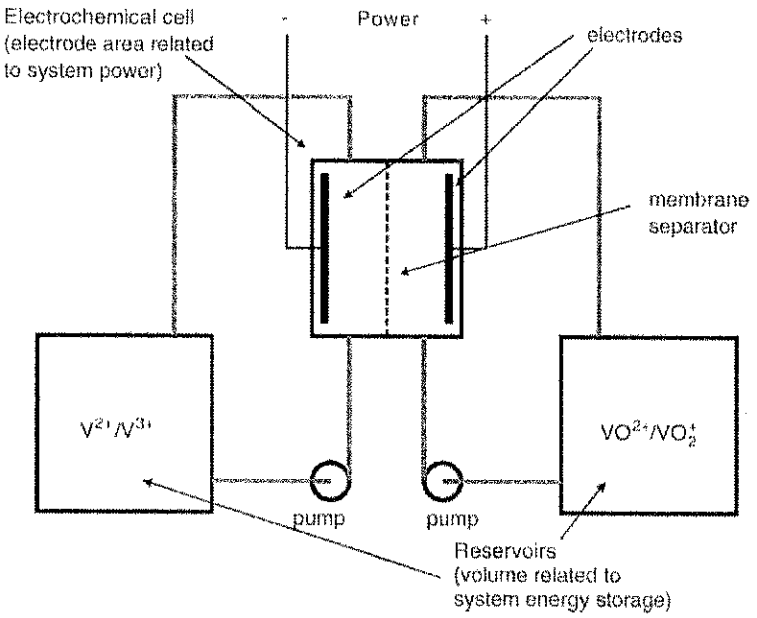

Fig. 1. A vanadium redox-flow battery (VRB) system.

Various approaches have been considered with significant efforts focused in the 70s on a system using Fe(II)/Fe(III) ($E_o = 0.771$ V versus SHE [5]) as the positive electrolyte and Cr(II)/Cr(III) ($E_o = -0.407$ V versus SHE [5]) as the negative electrolyte [6,7]. While this was not successful, due to problems related to the different species crossing the membrane and poor kinetics, more recent systems are now generating renewed interest. One uses polysulfur (S/S^{2-}) ($E_o = -0.476$ V versus SHE [5]) and bromine (Br^-/Br_3^-) ($E_o = 1.087$ V versus SHE [5]) [8] as the two electrolytes (being developed under the trade name Regenesys). Another uses V(II)/V(III) ($E_o = -0.255$ V versus SHE [5]) and halides such as bromine (Br^-/Br_3^-) ($E_o = 1.087$ V versus SHE [5]), which is characterised by a higher solubility of the reactants and so an improved energy density [9]. The system of interest in this work is the so called "all vanadium" flow battery, which uses vanadium V(II)/V(III) ($E_o = -0.255$ V versus SHE) and V(IV)/V(V) ($E_o = 0.991$ V versus SHE) [10,1,2]. The system makes use of the solubility of vanadium in four different oxidation states in strong acid conditions, to create a redox-flow battery using a single active chemical element (as shown in Fig. 1).

The overall reactions occurring at both electrodes during discharging of the VRB are typically written as shown below.

$$V^{2+} \rightleftarrows V^{3+} + e^- \quad (1)$$

$$VO_2^+ + e^- + 2H^+ \rightleftarrows VO^{2+} + H_2O \quad (2)$$

The polarisation curves for the two reactions are shown in Fig. 2. It can be seen that the kinetics of the V(IV) to V(V) reaction (Eq. (2)) are slower and more complex (see also [11]). It has been found in previous work [12], that by considering the three elementary steps of reaction (2) (i.e. one electron transfer and two proton exchanges), a reasonable fit can be obtained to the polarisation data. This detailed mechanism can involve three different possible pathways, and is shown in Fig. 3. The results of fitting the mechanism to polarisation data were consistent with the favoured mechanistic pathway changing depending on the pH and overpotential. An example of the fitted data is shown in Fig. 4A, with the contribution to the total current from each of the pathways shown in Fig. 4B. This mechanistic model could be used to fit polarisation curves over a range of pH, concentrations, and ratios of species. It can be seen, however, that the fit was not good for large overpotentials of the V(V) reduction reaction (see below 0.5 V in Fig. 4A). This region also corresponds to an unusual Tafel slope of greater than 460 mV $decade^{-1}$. Also, even if a low symmetry factor of less than 0.13 was used to fit the data below 0.5 V, the resulting calculated high Tafel polarisation curve would extend into the region near the reversible potential causing a poor fit in the 0.6–0.75 V region. One possibility raised in the previous work was that this result could be related to the low solubility of a $[VO_2 \cdot 4H_2O]^0$ intermediate species (on reaction pathway 3), which would be predicted to be produced in that potential region.

Accordingly, it is the purpose of this work to try to understand the reasons for the unusual Tafel slope and, in doing so, to develop a more complete understanding of the reaction mechanism. In terms of practical considerations, this high overpotential region is of interest at high rates of discharge. Such high overpotentials would, in particular, be encountered if high rates of discharge were demanded from a cell with a low state of charge (i.e. a low concentration of V(V)).

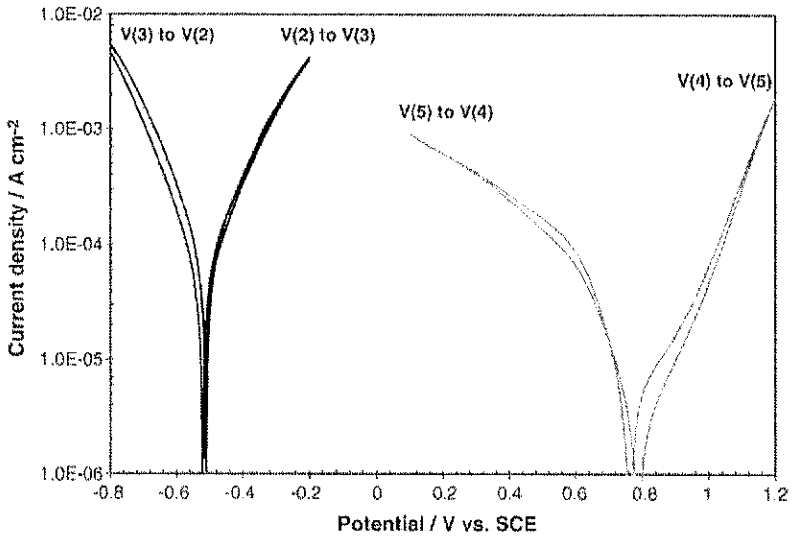

Fig. 2. Polarisation curves showing the two reactions used in a VRB (graphite electrode, 1 M H_2SO_4, 0.1 mV s^{-1}, 4000 rpm, 20 C. Left curve 16 mM V(2) and 36 mM V(3). Right curve 31 mM V(4) and 19 mM V(5)).

2. Experimental

The rotating disk system, including glassy carbon and pyrolytic graphite disc electrodes (0.196 cm^2), an AFMSRX electrode rotator, and the RDE cell (modified in house with a water jacket) was obtained from Pine Instruments. For most of the work, a cracked bead, low flow junction SCE reference (Fisher Scientific Accumet, <5 μL h^{-1} flowrate) was used to minimize possible solution contamination over long run times. A carbon rod pseudo-reference was used in parallel, connected via a series 10 μF capacitor, in order to decrease the reference electrode impedance and improve the potentiostat stability [17]. A glassy carbon plate counter electrode was used during experimental measurements. A similar, but separate, cell was used when running the electrodes in 1 M H_2SO_4, to avoid contamination.

The electrodes were initially hand polished with 600 and 1200 grit paper. Before each experiment they were then polished with a Buehler Ecomet 3 polisher at 100 rpm using a Nanocloth with 1, 0.3 and 0.05 μm alumina, followed by a thorough rinsing on the wheel (all using de-ionised water). This was followed by 5 min of ultrasound in acetone and 5 min in de-ionised water to remove polishing residues. It was found, however (as has also been reported by others [18]) that the activity of an electrode prepared in this manner drifted with time. It was felt that this was due to the freshly exposed carbon equilibrating with the electrolyte. Therefore, different methods were used to accelerate this process to obtain a reproducible surface.

One method involved an additional 5 min of ultrasound in a 40 mM V(5) 1 M H_2SO_4 solution. Another involved cycling the electrode 20 times between −0.1 and 1.1 V versus SCE in 1 M H_2SO_4. Both methods resulted in a slightly oxidised

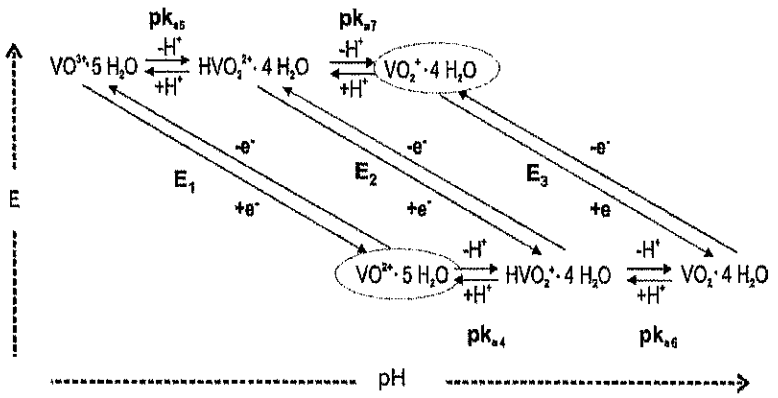

Fig. 3. The possible mechanistic pathways for the electrochemical reactions between V(4) and V(5) at low pH (note, that in strong sulphuric acid media, some of the water ligands may be replaced with sulphate or bisulphate [13–16]).

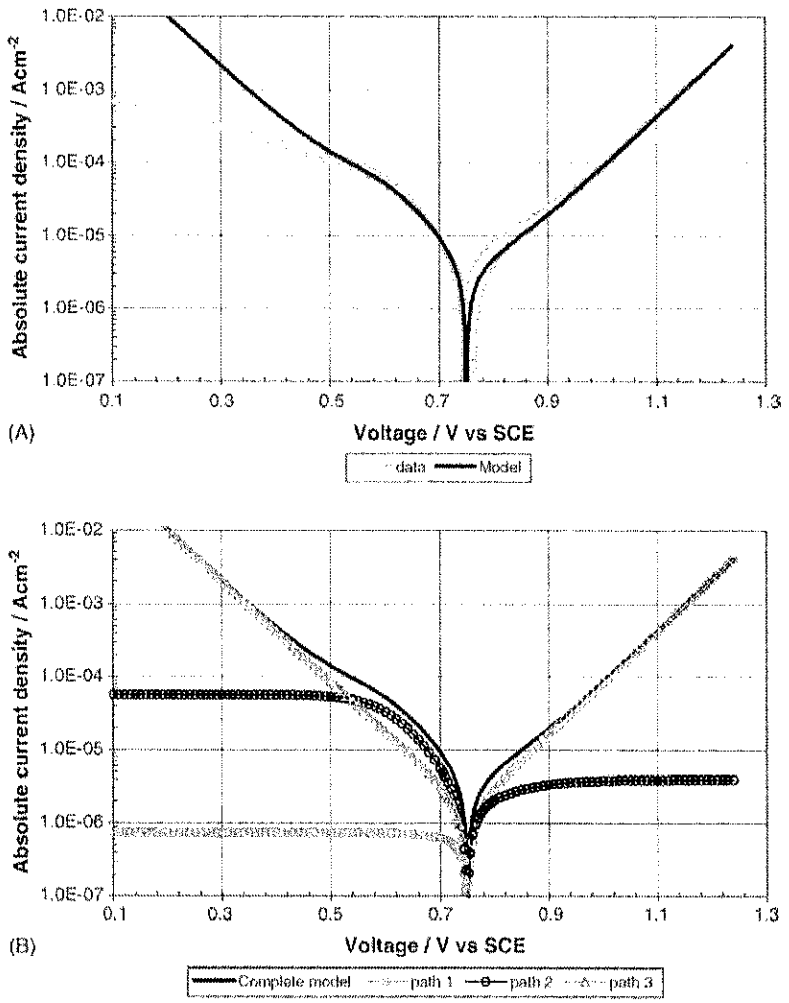

Fig. 4. Fitting polarisation data using the mechanistic pathways shown in Fig. 3. For the reduction reaction: Path 1 is CCE; Path 2 is CEC; and Path 3 is ECC (graphite electrode, 1.9 M H_2SO_4 + 1.4 M $KHCO_3$, 33 mM V(4), 17 mM V(5), 4000 rpm, 0.2 mV s^{-1}).

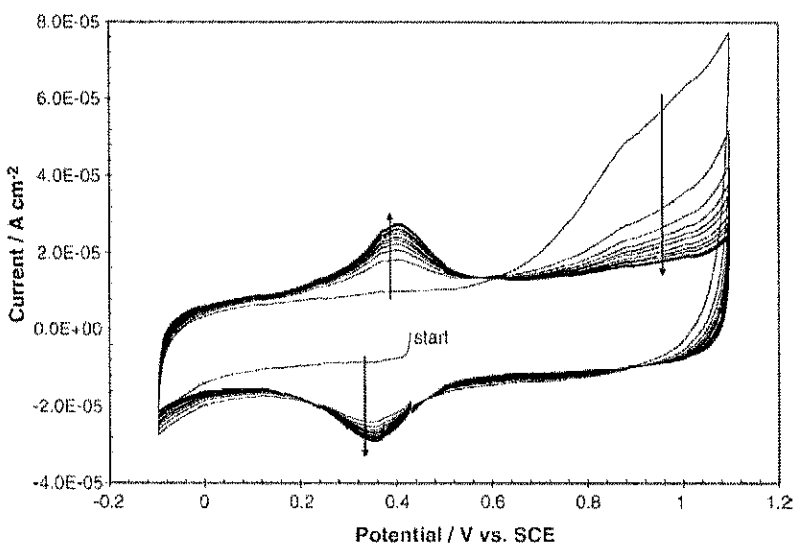

Fig. 5. The initial voltammetric cycles for a freshly prepared graphite electrode (100 mV s^{-1}, 1 M H_2SO_4, 20 cycles shown).

surface. This could be clearly seen in the second approach (shown in Fig. 5), where the first cycle showed essentially no peaks due to surface quinine groups, but a significant oxidation current starting around 0.6 V (where surface phenol groups might be expected to be oxidized). As the cycles progressed, the oxidation current decreased and the current due to surface quinine groups increased (the pair of peaks centred on 0.39 V).

A third method, that has been more recently adopted, involved etching the post polished surface by anodic polarisation in caustic solution (1.8 V in 0.1 M NaOH, 20 s for glassy carbon and 1.7 V for 10 s for pyrolytic graphite). This has been reported to remove carbon powder residue from polishing, which is not removable by ultrasound [19]. This, however, also results in a surface with a relatively low oxidation state (thought to be due to the stronger relative rate of corrosive attack on higher oxidation state surface sites by the caustic solution [20,21]). Accordingly, this surface etching was also followed by cycling the electrode 20 times between −0.1 and 1.1 V versus SCE in 1 M H_2SO_4 to produce a stable surface. This method resulted in noticeably more reproducible results from day to day and more stable results from cycle to cycle.

The electrochemical measurements were carried out using an EG&G 263 potentiostat with Scribner CorrWare and CorrView 2.80 data collection and analysis software. The chemicals used include $VOSO_4$ and V_2O_5 from Alfa Aesar (with certificates of analysis showing <99.9% and 99.6% respective purity on a metals basis), ACS grade H_2SO_4, $HClO_4$, and Na_2CO_3 from EM Science, and de-ionized water from a Millipore Milly-Q Plus system.

Removing dissolved oxygen by sparging the solutions with argon was observed to have no effect on the V(4)/V(5) couple. Because of possible contamination from the SCE electrode, a test was carried out where chloride was added to the cell (ca 10–20 mg to 200 mL solution), which resulted in no significant change to the voltammetry.

3. Results and discussion

3.1. General testing

Because the very high Tafel slope could be related to mass transport limitations, measurements were made at various rotation rates of the rotating disk electrode. The results are shown in Fig. 6, with the effect of rotation rate becoming significant at potentials below 0.1 V (and above 1.2 V). Note that below 0.1 V versus SCE, there is the possibility of the reduction of V(4) to V(3) (E_o = 0.337 V versus SHE [22]), though this reaction is reported to be quite slow [23,24]. Thus, within the range of potentials shown in Fig. 4, there is little effect of solution phase mass transport. Using the Levich equation, one can also confirm that the limiting current plateau probably occurs around −0.2 to −0.3 V. For example, the estimated limiting current using 4000 rpm, 29 mM V(5), kinematic viscosity = 0.01 $cm^2\ s^{-1}$ and diffusion coefficient = $3 \times 10^{-6}\ cm^2\ s^{-1}$, is 16 mA cm^{-2}. The unusual shape of the cathodic polarisation curve is related to the change in the Tafel slope occurring at around 0.5 V, visible in Fig. 2.

The effect of pH on the reaction rate was also measured. As can be seen in Fig. 7, the reaction is independent of pH in the high Tafel slope region. Thus, the reaction in the high Tafel slope region appears to be consistent with the following mechanism (from Fig. 3):

$$[VO_2 \cdot 4H_2O]^+ + e^- \rightleftarrows [VO_2 \cdot 4H_2O]^0 \quad \text{r.d.s.} \tag{3}$$

$$[VO_2 \cdot 4H_2O]^0 + H^+ \rightleftarrows [VOOH \cdot 4H_2O]^+ \tag{4}$$

$$[VOOH \cdot 4H_2O]^+ + H^+ \rightleftarrows [VO \cdot 5H_2O]^{2+} \tag{5}$$

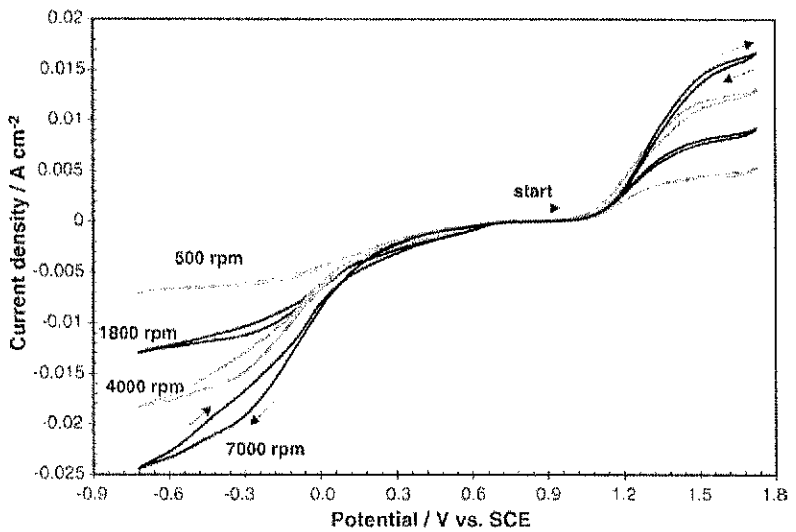

Fig. 6. Effect of rotation rate (graphite electrode, 10 mV s^{-1}, 1 M H_2SO_4, 21 mM V(4), 29 mM V(5)).

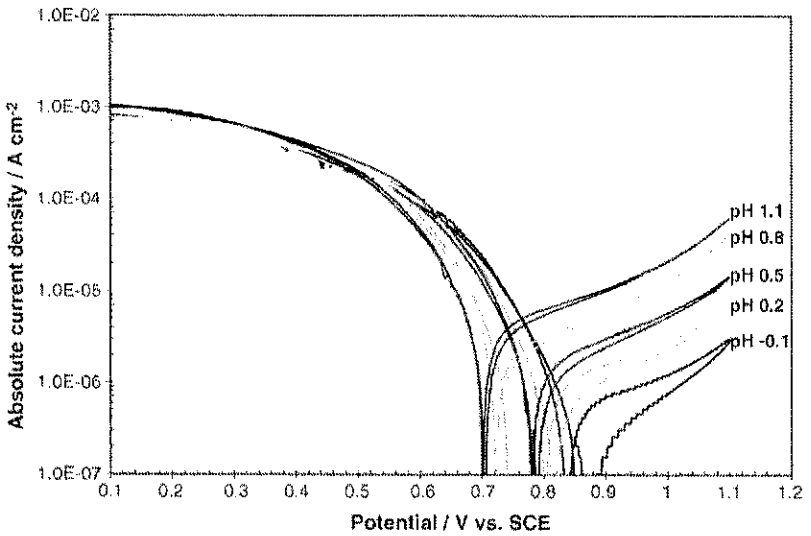

Fig. 7. Polarisation curves at various values of pH (pH 0.1: 1.25 M $HClO_4$; pH 0.2: 0.625 M $HClO_4$ + 0.625 M $NaClO_4$; pH 0.5: 0.313 M $HClO_4$ + 0.937 M $NaClO_4$; pH 0.8: 0.156 M $HClO_4$ + 1.094 M $NaClO_4$; pH 1.1: 0.078 M $HClO_4$ + 1.172 M $NaClO_4$ (graphite electrode, 1 mV s^{-1}, 40 mM V(5), 10 mM V(4), 4000 rpm).

(Though, it should be noted that, it is likely that in sulphuric acid solution some of the ligands may be replaced with sulphate or bisulphate). Such a mechanism leads to speculation that the postulated intermediate, VO_2^0, which would be expected to have a low solubility, is a cause of the observed high Tafel slope.

If a poorly soluble intermediate such as VO_2^0 is considered to cause the low apparent symmetry factor, this could involve a precipitated film that limits mass transport or causes a high resistive drop. However, in these cases a critical local saturated concentration of the intermediate, related to a critical flux, might be expected. It should then be possible to find a reactant concentration low enough to avoid precipitation or complete coverage of the electrode surface. Tests were therefore done to see the effect of the reactant concentration over a range from 0.03125 to 280 mM, with the results shown in Fig. 8. It is interesting to note that there does not seem to be a critical current density (or flux) at which the low Tafel slope begins. Potential step measurements also did not show the current decay characteristic of diffusion through a deposited film (i.e. a current decay with square root of time) nor of sufficient magnitude to account for the suppressed current in the high Tafel region. Further, a precipitated film limiting access of reactant to the electrode should result in a steady-state current where the film growth is equal to the film dissolution, hence potential independent. In additional tests,

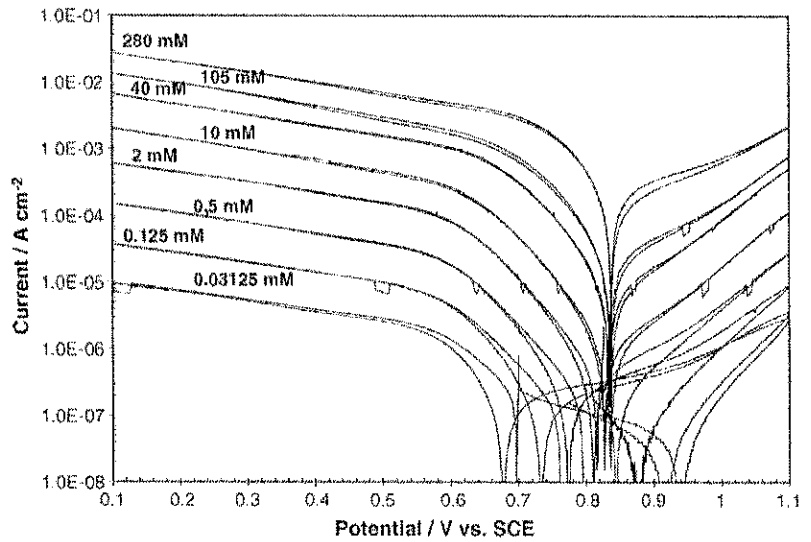

Fig. 8. Polarisation curves over a range of vanadium (5) concentrations (graphite electrode, 1 mV s^{-1}, 1 M H_2SO_4, 4000 rpm, V(4) concentration at 25% of V(5)).

measurements using the IR interrupt function on the 263 potentiostat also showed no measurable increase in resistance in the high Tafel slope region. This rules out the possibility of a resistive film being deposited on the electrode surface. (It can be seen in Fig. 4A, that for a resistive drop to account for the difference between the observed Tafel slope and a more typical 120 mV decade^{-1} Tafel slope, would require an easily measured IR drop of a few hundred millivolts.)

3.2. Carbon surface effects

Another possibility is that the low apparent symmetry factor is due to changes in the carbon electrode surface. Referring to Fig. 5, the surface quinone groups undergo reaction at around 0.39 V, which is mid-point of the measured high Tafel region. Thus, if the carbon surface with reduced, catechol-type surface groups, has a lower activity than the surface with oxidised, *o*-benzoquinone-type groups, then a decreasing activity with more cathodic potential might occur, leading to a low apparent symmetry factor.

To test this idea, a freshly etched carbon electrode that has not been subjected to anodic cycling (and thus has a relatively un-oxidised surface as discussed in Section 2) was used. Further, a special low redox potential solution (i.e. a low ratio of V(5)–V(4)) was also used to avoid oxidising the surface at open circuit prior to measurement of the un-oxidised surface polarisation curve. The results are shown in Fig. 9. This electrode gave repeated cycles with a very straight Tafel region and a very low transfer coefficient of only 0.082 (733 mV decade^{-1} with a correlation coefficient of 0.9994). This was followed by polarisation cycles that continued up to 1.1 V, where the carbon surface would become oxidised (see Fig. 5). For the oxidised surface, hysterisis is observed and the current is lower at most potentials versus the low oxidation case. However, as the surface *o*-benzoquinone-type groups change from oxidised to reduced state (centred on 0.39 V), the polarisation curve begins to bend upward to join the curve for the un-oxidised surface. Thus, the presence of surface *o*-benzoquinone-type groups suppresses the reaction rate, though the reaction rate is largely recovered when these groups are reduced to their catechol-type form, and hysterisis is observed as this "recovered" reaction rate is retained on the reverse sweep.

Thus, the type of surface oxide functional group on the carbon was found to have a clear effect on the voltammetric curves (again showing the strong surface sensitivity of this reaction). However, rather than being the cause of the low apparent symmetry factor, the effect for typical polarisation curves is actually to increase the apparent symmetry factor.

3.3. Adsorbed intermediates

As well as the effect of the state of oxidation of the carbon surface on the reaction, we have found large differences in reaction rate with the type of carbon (glassy carbon versus pyrolytic graphite [25]). Other workers have found differences with the surface polishing [18] and with different preparations and types of carbon felt electrodes [26,27]. This is typical of an inner Helmholtz layer type reaction, and so a full understanding of the reaction should also consider the role of adsorbed intermediates. If the reaction involves adsorption, one could break down the reaction of Eq. (3) into three steps.

$$VO_2^+ \rightleftarrows VO_{2\,ads}^+ \tag{6}$$

$$VO_{2\,ads}^+ + e^- \rightleftarrows VO_{2\,ads}^0 \tag{7}$$

$$VO_{2\,ads}^0 \rightleftarrows VO_2^0 \tag{8}$$

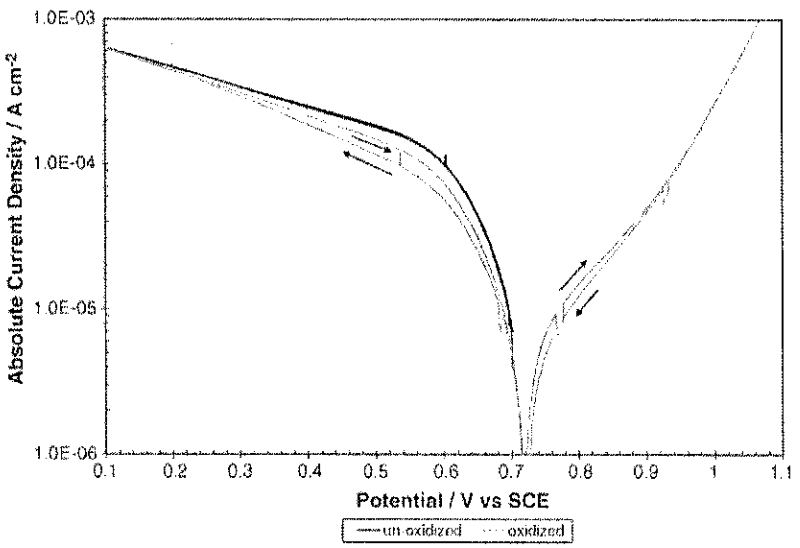

Fig. 9. Different results for an "as prepared carbon surface" (low oxidation state) and an "oxidised carbon surface" (cycled to 1.1 V) (graphite electrode, 1 mV s^{-1}, 1 M H_2SO_4, 2 mM V(5) and 48 mM V(4), 4000 rpm).

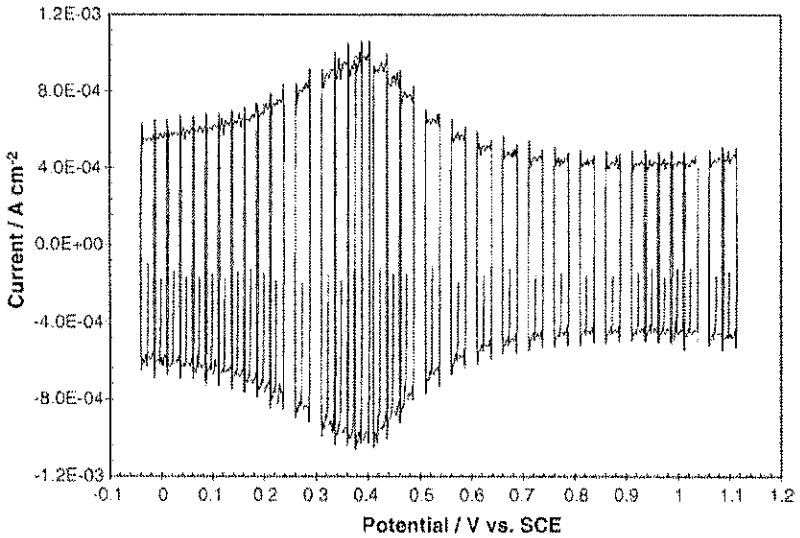

Fig. 10. Electrode double layer capacitance measurement results (graphite electrode, 1 M H_2SO_4, 5000 mV s^{-1}).

(Note that a step such as $VO^0_{2\,ads} + H^+ \rightleftarrows VOOH^+$ would, if it was rate determining, lead to a pH dependence that would not be compatible with the results in Fig. 7).

To investigate possible adsorbed intermediates, the electrode capacitance was measured using a sawtooth waveform with an amplitude of 30 mV and a sweep rate of 5000 mV s^{-1}. This is similar to the method suggested in the literature for measuring carbon double layer capacitance [20,28]. This method offers the advantage of a very short test time (a 3 min hold at the centre potential, followed by 36 ms for three test cycles). This allows a range of potentials to be measured with fewer concerns about changes in the state of the electrode surface over the course of the measurements. A typical result for pyrolytic graphite in sulphuric acid is shown in Fig. 10.

The results in Fig. 10 clearly show a large pseudocapacitance around 0.39 V related to carbon surface quinone species [20]. Following the blank test in sulphuric acid, the electrode was transferred to a vanadium containing solution where the double layer sweep test was repeated, a slow (1 mV s^{-1}) polarisation curve was measured, and the double layer sweep test was repeated. After this, the electrode was removed, rinsed and the blank test in sulphuric acid was repeated. Results in the presence of vanadium are shown in Fig. 11. From these results, plots of capacitance versus voltage can be made as shown in Fig. 12.

On comparing the results with and without vanadium, several changes in electrode capacitance are observed. The pseudocapacitance related to the surface quinone groups is

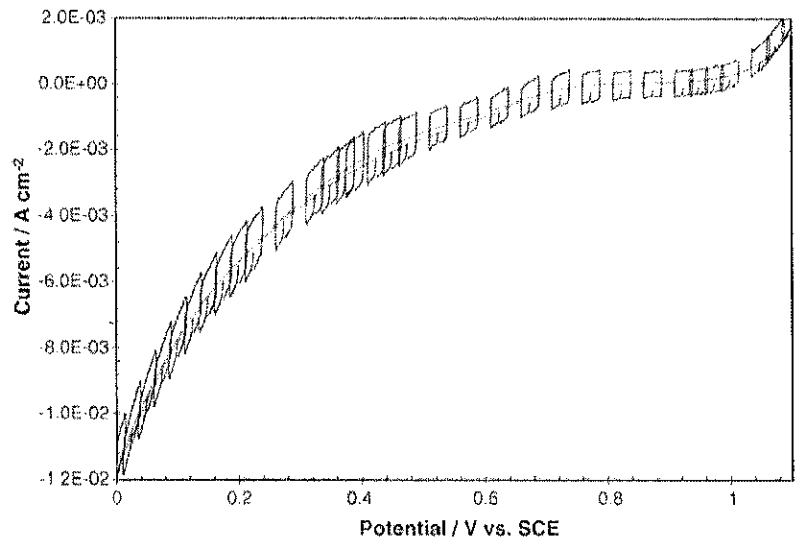

Fig. 11. Electrode double layer capacitance measurement results with vanadium present. Steady state result for a 1 mV s^{-1} sweep also shown in grey (graphite electrode, 1 M H_2SO_4, 42 mM V(5), 42 mM V(4), 4000 rpm).

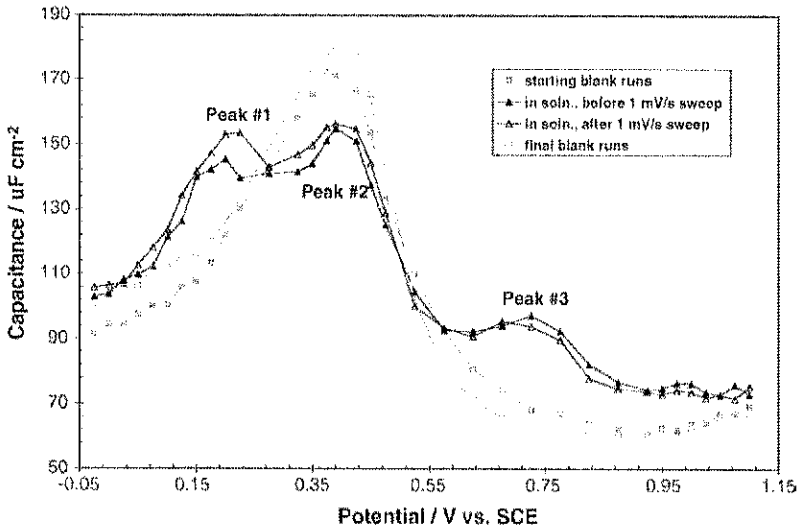

Fig. 12. Plot of capacitance versus voltage for a pyrolytic graphite electrode using the data in Figs. 10 and 11.

significantly diminished. Also, two new pseudocapacitance peaks appear, one at about 0.175–0.2 V (Peak 1), and the other about 0.675–0.725 V (Peak 3). These changes were reversed on returning the electrode to a vanadium free, sulphuric acid solution. Similar tests were carried out for a range of total vanadium concentrations and for different ratios of V(4)–V(5). Note that for measurements at higher concentrations (greater than 40 mM V(5)) and higher overpotentials (e.g. less than 0.3 V) the resulting lower Faradaic resistance (R_f) makes the influence of IR drop errors on the capacitance measurement larger, i.e.:

$$C_{\text{apparent}} = C\left(\frac{R_f}{R_f + R_S}\right)^2 \quad (9)$$

The use of IR correction can be used to extend the measurement range somewhat, before errors become too large. Because of the high sweep rates used, positive feedback IR correction was used, with the resistance value (R_S) evaluated using the potentiostat's in-built current interruption and an oscilloscope.

One result of these tests was that the observed changes in the presence of vanadium correlated to the concentration of V(5), independent of the V(4) concentration. The different peaks also have different concentration dependencies (from 0.03125 to 280 mM V(5)) and sweep rate dependencies (from 20 to 10000 mV s^{-1}). The effect of concentration is shown in Fig. 13. Peak 1 appeared at V(5) concentrations above 0.5 mM with a capacitance that increased steadily with lower

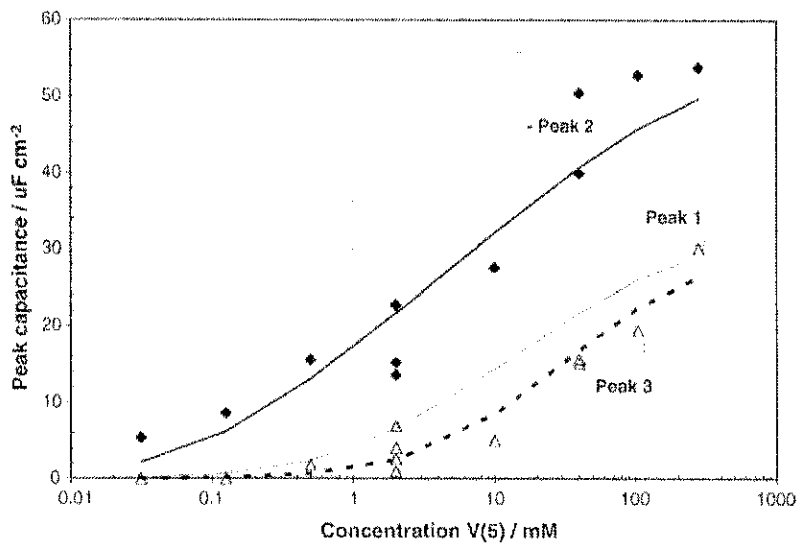

Fig. 13. Relationships found between V(5) concentration and the measured pseudocapacitance peak heights (note, curves are shown simply for ease of seeing data trends).

sweep rate. The suppression of Peak 2 occurred in the lowest tested V(5) solution (0.03125 mM) and was relatively independent of sweep rate. This would appear to indicate that there is a strong interaction between V(5) and the carbon surface quinone groups. Peak 3 appeared at V(5) concentrations above 2 mM with a capacitance that increased as the sweep rate was lowered to around 500 mV s^{-1}, then remained relatively constant. In all three cases the dependence with concentration was not linear, being better represented by a Langmuir or Temkin type relationship.

It is interesting to compare these results with the mechanism proposed in our previous paper (shown in Fig. 3). In that work, for the purpose of trying to fit experimental data with a model, estimates had been made for the various pK_a and E_o values. From the literature $E^o{}_{overall} = 1.004$ V versus SHE (0.763 V versus SCE) and p$K_{a4} = 5.36$ [22]. Values for the other equilibrium constants are not available and so, in the previous work, to see the quality of the qualitative fit to the data, approximate values for the various pK_as were used. The existence of $HVO_2{}^{2+}$ has been suggested from the variation of the equilibrium potentials of V(IV)/V(V) mixtures in strong acid [29], but no stable $HVO_2{}^{2+}$ species is reported above pH −1 [22]. Therefore, values of p$K_{a7} = -2$ and p$K_{a5} = -3$ were chosen. Data for the equilibrium between VO^{2+} and V_2O_4 is available, but not for VO_2. The value of pK_{a6} must be more alkaline than pK_{a4}, but from Pourbaix, the equilibrium between 1 mM VO^{2+} and the dry oxide V_2O_4 would occur at pH 3.95 [22]. Thus a value slightly more alkaline than pK_{a4}, of p$K_{a6} = 5.6$, was chosen. Based on these values, E_o values can be estimated. This is because for each path the overall free energy changes must be the same. Therefore, each E^o can be specified in terms of an overall E^o as shown below:

$$nFE^o_{overall} = nFE^o_1 - RT\ln(K_{5eq}K_{7eq}) \quad (10)$$

$$nFE^o_{overall} = nFE^o_2 - RT\ln(K_{4eq}K_{7eq}) \quad (11)$$

$$nFE^o_{overall} = nFE^o_3 - RT\ln(K_{4eq}K_{6eq}) \quad (12)$$

This resulted in estimated values of $E_{o1} = 1.05$ V, $E_{o2} = 0.57$ V, and $E_{o3} = 0.13$ V (all versus SCE). It is interesting to note that the potential of E_{o2} is similar to that of Peak 3 and E_{o3} to that of Peak 1. (Note that, even if the above pK_a estimates were correct, there would be some discrepancy due to the, probably different, energies of adsorption of the various species and the possibility that the observed reactions are displaced from equilibrium. On the other hand, an error of 1 pH unit in an assumed pK_a would only result in an error of 0.06 V in the estimated E_o.)

As there obviously are adsorbed intermediates, we can return to Eqs. (6)–(8) to see what would be predicted. Because the measured pseudocapacitance in the presence of $VO_2{}^+$ indicates the presence of adsorbed intermediates, it is unlikely that step 6 would be rate determining. If step 6 is at equilibrium, we can write (assuming the simplest case of a Langmuir isotherm) that coverage of adsorbed $VO_2{}^+$ is given by:

$$\theta_{VO_2^+} = \frac{[VO_2^+]k_{6f}(1 - \theta_{VO_2^0})}{[VO_2^+]k_{6f} + k_{6r}} \quad (13)$$

And, assuming steady state, one can write for the coverage of adsorbed VO_2^0:

$$\frac{d\theta_{VO_2^0}}{dt} = \theta_{VO_2^+}k_7 \exp\left(\frac{-\alpha F}{RT}(V - E'_o)\right) - \theta_{VO_2^0}k_7 \exp\left(\frac{(1-\alpha)F}{RT}(V - E'_o)\right) - \theta_{VO_2^0}k_8 = 0 \quad (14)$$

Then the coverage of VO_2^0 would be:

$$\theta_{VO_2^0} = \frac{\theta_{VO_2^+}k_7 \exp\left(\frac{-\alpha F}{RT}(V - E'_o)\right)}{k_8 + k_7 \exp\left(((1-\alpha)F/RT)(V - E'_o)\right)} \quad (15)$$

This predicts that when:

$$k_8 < k_7 \exp\left(\frac{(1-\alpha)F}{RT}(V - E'_o)\right)$$

Then step 8 will be rate determining and step 7 will be close to equilibrium:

$$\theta_{VO_2^0} = \theta_{VO_2^+} \exp\left(\frac{-F}{RT}(V - E'_o)\right) \quad (16)$$

At very high overpotentials the coverage of VO_2^0 would become essentially 1 and the reaction rate would be potential and concentration independent. There is no sign of such an occurrence in the data shown in Fig. 8. For lower VO_2^0 coverages the reaction rate, if step 8 is rate determining, is given by:

$$\frac{i}{nF} = \theta_{VO_2^0}k_8 = \theta_{VO_2^+}k_8 \exp\left(\frac{-F}{RT}(V - E'_o)\right) \quad (17)$$

And when:

$$k_8 > k_7 \exp\left(\frac{(1-\alpha)F}{RT}(V - E'_o)\right)$$

Then step 7 is rate determining and the reaction rate is:

$$\frac{i}{nF} = \theta_{VO_2^+}k_7 \exp\left(\frac{-\alpha F}{RT}(V - E'_o)\right) \quad (18)$$

Therefore, above a transition potential the transfer coefficient should be 1 (Eq. (17)), and below the transition potential the transfer coefficient should be α (Eq. (18)), as is typical for an EC type mechanism. This does generally fit the observed data, for example the results in Fig. 8, but has a couple of discrepancies. One is that it does not explain why the symmetry factor should be so low. A second problem is that the transition potential, where the rate determining step changes, occurs at a potential significantly anodic to the expected equilibrium potential. In Fig. 8 the mechanism change appears around 0.6 V for most of the polarisation curves. (The

deviation at higher concentrations may be due to the formation of vanadium complexes such as $V_2O_3^{3+}$ [30]). Using the estimated equilibrium potential of $E'_0 = 0.13$ V one can then state at the transition potential:

$$k_8 = k_7 \exp\left(\frac{(1-\alpha)F}{RT}(V - E'_0)\right)$$

$$= k_7 \exp\left(\frac{(1-\alpha)F}{RT}(0.6 - 0.13)\right) \approx k_7 9430 \quad (19)$$

Then, at the equilibrium potential, around where the coverage of θ_5 should be changing to θ_4 at the highest rate, and so where the peak pseudocapacitance should be seen, using Eqs. (15) and (19) one obtains:

$$\theta_{VO_2^0} = \frac{\theta_{VO_2^+} k_7}{k_7 9430 + k_7} = \frac{\theta_{VO_2^+}}{9431} \quad (20)$$

This makes it difficult to see how a significant pseudocapacitance would occur at the potential of Peak 1. Note a symmetry factor of 0.5 was used in the calculation. Using 0.13 would yield an even lower coverage of VO_2^0 at the equilibrium potential. Thus, it appears that the pseudocapacitance data (related to adsorbed intermediates) is not consistent with the steady-state polarisation data (related to VO_2^+ from the solution undergoing reaction at the electrode).

3.4. A reaction model

One common explanation for a low apparent symmetry factor is that only some fraction of the applied potential is actually driving the rate determining step [31]. We, therefore, considered the situation where there might be a strongly adsorbed layer of reaction intermediates on the electrode surface, with the electron transfer occurring through that layer to reactant further from the electrode. This two layer model would also help to explain the apparent discrepancy between the pseudocapacitance data and the steady state polarisation data.

In such a case, the shape of the electric field near the electrode surface will affect the electron transfer to the adsorbed layer and to reactant further from the electrode. In the reaction being considered in this work, the adsorbed layers appear to reach their maximum pseudocapacitance at close to what might be the expected values (i.e. close to the postulated equilibrium potentials). On the other hand, the overall reaction displays an extremely low apparent symmetry factor. These results would therefore correspond to the situation where most of the potential drop activates electron transfer from the electrode to the adsorbed layer, with relatively little remaining to activate the electron transfer to reactant located further from the electrode. Thus, we would postulate an inner strongly adsorbed layer where k_8 is small and most of the applied potential drop occurs. This would give rise to the observed pseudocapacitance, but because of the low turn over, it would only have a small contribution to the observed steady state reaction rate. A second, less strongly adsorbed layer

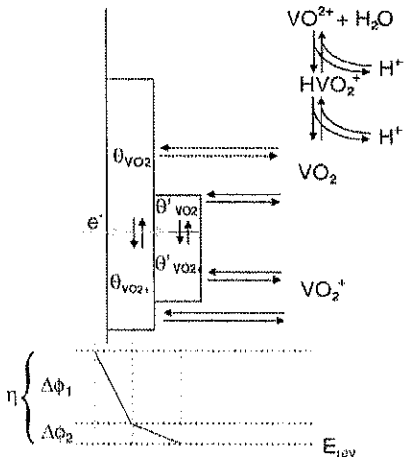

Fig. 14. A two layer model of adsorbed intermediates at the electrode surface with the postulated potential drop.

(i.e. with a larger k_8) would have a high turn over and a more anodic transition potential, along with a smaller fraction of the applied potential and so a low apparent symmetry factor. This second, higher turnover, layer would produce the reaction current observed in the polarisation curves. This model is diagrammed in Fig. 14.

In the model, reactions in both layers involve adsorption. This is because, if the main reaction measured in the polarisation curves were outer Helmholtz, a more normal symmetry factor (i.e. near 0.5) would be expected at open areas of the electrode. This would be expected to be especially apparent at low concentrations where a large part of the electrode surface would be uncovered (the fact that the surface is not saturated is supported by the pseudocapacitance results varying with concentration in Fig. 13). The assumption of an inner Helmholtz reaction is also supported by other electrochemical studies of non-complexed metal ions at carbon. In particular, it is thought that interaction with surface oxygen groups is important to obtain reasonable reaction rates [32–34]. In the model in Fig. 14, the second layer would, however, be adsorbing on an inner layer of adsorbed vanadium. While such an adsorption is postulated to be weaker (i.e. a higher k_8), some catalysis may occur through interaction with the inner adsorbed layer. The interactions of vanadium with oxygen containing species, and with other vanadium oxides to form polymetaloxylates, are both well known [35,36]. Also, in such a case, as the reactant concentration is changed, both layers would proportionally change in relation to their different isotherms. This would result in a reactive structure on the electrode surface that would remain generally similar over a range of conditions and so might more easily explain the consistent data in Fig. 8. Also, in this model the presence of a blocking layer of adsorbed intermediates is related to the expected low solubility of an adsorbed VO_2^0 intermediate. This explanation is therefore also consistent with the lack of such an unusual transfer coefficient for the VO^{2+} to VO_2^+ reaction (which involves the same reactant

and product species, but does not have the same intermediate [12]).

While such a model appears to qualitatively fit with the observed data, there are many details that need to be determined in terms of the exact film structure and mechanism of electron transfer. The tunnelling of electrons through an adsorbed bridge species has been theoretically analysed by Dogonadze et al. [37,38] and Schmickler [39]. Dogonadze et al. have developed models for the case where the adsorbed intermediate is present at small coverage and hence has a discrete electronic spectrum [37] and for the case of high coverage where the bridge species is represented by a quasi-continuous surface energy band [38]. A second distinction was based on whether most of the applied electric field appears across the electrode-bridge step or the bridge-solution ion step. The resulting models gave predictions that could include a symmetry factor of close to or equal to zero. In Schmickler's work the electron transfer was considered from the electrode, through the bridge, to the solution species as a single tunnelling event. The electron transfer requires the system to reorganise so that the electronic energies of the initial, intermediate, and final states are equal. It is felt that the predicted current-potential curves will be complex as the electronic energies of the surface state and the redox couple would likely be dependent on the overpotential. Thus, the predictions of both models are sensitive to the shape of the electric field across the adsorbed layer.

If a second layer can adsorb on the first vanadium layer, then possibly a third layer could adsorb on the second layer, and so a wedding cake type multilayer film might also be possible. In such a case, the movement of electrons through the film might be better described by electron hopping theory. Another consideration is how the changes in surface coverages of adsorbed species with potential might effect the apparent Tafel slope. For example, if the desorption of the VO_2^0 intermediate is slow (Eq. (8)) and the electrochemical reaction (Eq. (7)) is close to equilibrium, the ratio of the coverage of the adsorbed VO_2^0 intermediate versus adsorbed VO_2^+ would be expected to follow a Nernst relationship. It is not clear how such changes to the inner adsorbed layer might affect the second layer and the electron transfer. Thus, while the two layer model does show promise in explaining the data obtained to date, much still needs to be better understood to say if the model is correct.

In such a model, the adsorbed intermediate's structure and so the overall response might be expected to be influenced by changes to the electrode surface and also possibly the electrolyte. Some indication of this can be seen on comparing the shape of the polarisation curves measured in sulphuric acid (Fig. 8) with those in perchloric acid (Fig. 7). Thus, while the observed polarisation curves for VO_2^+ reduction are consistent across a range of pH values and a very wide range of concentrations, they are very sensitive to the state of the surface and the anions used. Finally, it is interesting to note in the work of Oriji et al. [16], that the voltammetric peak for the V(5)–V(4) reaction becomes much more reversible as the sulphuric acid concentration is changed from 1 to 9 M, indicating that the situation might also change in high ionic strength solutions.

4. Conclusions

An investigation has been carried out to try to determine the reason behind the low apparent symmetry factor found when reducing VO_2^+ at high overpotentials at a carbon electrode. The low apparent symmetry factor was found to occur with both glassy carbon and pyrolytic graphite, over a wide range of reactant concentrations, and pH values from 0 to 1. This does not appear to be due to mass transport limitations, a precipitated film, or adsorption or desorption rate determining steps.

Double layer measurements made while the reaction was occurring showed two peaks that increased with increasing concentration of VO_2^+. Also the typical carbon electrode pseudocapacitance, due to the reversible oxidation and reduction of surface quinone type oxygen groups, was suppressed in the presence of even very low concentrations of VO_2^+. An increasing suppression was observed with increasing VO_2^+ concentration.

A number of theories to explain the low apparent transfer coefficient for the reduction of VO_2^+ have been considered, but none have been able to explain the data obtained to date. At present, the best theory involves electron transfer to the reacting species through a layer of adsorbed intermediates that are slow to desorb from the electrode surface. Because of this, the entire applied potential is not available to drive the rate determining step, leading to the observed low apparent symmetry factor. While more work is needed to completely verify and detail this theory, it shows promise in helping understand the data obtained to date and in focusing further research. Thus, the present research has helped to increase the understanding of this complex, but important, electrochemical system.

Acknowledgements

The authors would like to thank Prof. Eliezer Gileadi for helpful discussions and Stephanie McCarthy for collecting some of the data used in this paper.

References

[1] M. Skyllas-Kazacos, An historical overview of the vanadium redox flow battery development at the University of New South Wales, Australia, in: M.F. Taner, P.A. Riveros, J.E. Dutrizac, M.A. Gattrell, L.M. Perron (Eds.), Vanadium—Geology, Processing and Applications, Canadian Institute of Mining, Metallurgy and Petroleum, Montreal, 2002, p. 95.

[2] S. Miyake, N. Tokuda, Development and application of the vanadium redox-flow battery, in: M.F. Taner, P.A. Riveros, J.E. Dutrizac, M.A. Gattrell, L.M. Perron (Eds.), Vanadium—Geology, Processing and Applications, Canadian Institute of Mining, Metallurgy and Petroleum, Montreal, 2002, p. 95.
[3] R.M. Dell, D.A.J. Rand, J. Power Sources 100 (2001) 2.
[4] EPRI-DOE Handbook of Energy Storage for Transmission and Distribution Applications, EPRI, Palo Alto, CA and the U.S. Department of Energy, Washington, DC, Report #1001834, 2003.
[5] D.R. Lide (Ed.), CRC Handbook of Chemistry and Physics, CRC Press, Boca Raton, FL, 1999.
[6] L.H. Thaller, "Electrically rechargeable redox flow cell", U.S. Patent 3,996,064, 7 December (1976).
[7] J. Giner, L. Swette, A. Cahill, "Screening of Redox Couples and Electrode Materials", CR 134705, for NASA-Lewis Research Center, Cleveland, Ohio, September 1976.
[8] R.J. Remick, P.G.P. Ang, U.S. Patent 4,485,154, 27 November (1984).
[9] M. Skylass-Kazacos, J. Power Sources 124 (2003) 299.
[10] M. Skyllas-Kazacos, M. Rychick, R. Robins, "All-Vanadium redox battery", U.S. Patent 4,786,567, 27 November (1988).
[11] S. Zhong, M. Skyllas-Kazacos, J. Power Sources 39 (1992) 1.
[12] M. Gattrell, J. Park, B. MacDougall, J. Apte, S. McCarthy, C.W. Wu, J. Electrochem. Soc. 151 (1) (2004) 123.
[13] N. Kausar, R. Howe, M. Skyllas-Kazacos, J. Appl. Electrochem. 31 (2001) 1327.
[14] X. Lu, Electrochim. Acta 46 (2001) 4281.
[15] A.A. Ivakin, E.M. Voronova, Russ. J. Inorg. Chem. 18 (7) (1973) 956.
[16] G. Oriji, Y. Katayama, T. Miura, Electrochim. Acta 49 (2004) 3091.
[17] "Technical Note 200—Potentiostat Stability Considerations", EG&G Princeton Applied Research.
[18] E. Sum, M. Rychcik, M. Skyllas-Kazacos, J. Power Sources 16 (1985) 85.
[19] G.K. Kiema, M. Aktay, M.T. McDermott, J. Electroanal. Chem. 540 (2003) 7;
G.K. Kiema, G. Fitzpatrick, M.T. McDermott, Anal. Chem. 71 (1999) 4306.
[20] R.L. McCreery, Carbon Electrodes: Structural effects on electron transfer kinetics, in: A.J. Bard (Ed.), Electroanalytical Chemistry, 17, Marcel Dekker, Inc., New York, 1991, p. 221.
[21] C. Kozlowski, P.M.A. Sherwood, J. C. S., Faraday Trans. I 81 (1985) 2745.
[22] M. Pourbaix, Atlas of Electrochemical Equilibria in Aqueous Solutions, second ed., NACE, Houston, 1974, p. 234.
[23] Y. Isreal, L. Meites, J. Electroanal. Chem. 8 (1964) 99.
[24] E. Barrado, R. Pardo, Y. Castrillejo, M. Vega, J. Electroanal. Chem. 427 (1997) 35.
[25] M. Gattrell, J. Park, B. MacDougall, S. McCarthy, J. MacDonald, The impact of low temperature on vanadium redox battery (VRB) performance, in: M.F. Taner, P.A. Riveros, J.E. Dutrizac, M.A. Gattrell, L.M. Perron (Eds.), Vanadium – Geology, Processing and Applications, Canadian Institute of Mining, Metallurgy and Petroleum, Montreal, 2002, p. 79.
[26] B. Sun, M. Skyllas-Kazacos, Electrochim. Acta 37 (7) (1992) 1253.
[27] B. Sun, M. Skyllas-Kazacos, Electrochim. Acta 37 (13) (1992) 2459.
[28] N. Tshernikovski, E. Gileadi, Electrochim. Acta 16 (1971) 579.
[29] Y. Isreal, L. Meites, Vanadium, in: A.J. Bard (Ed.), Encyclopaedia of Electrochemistry of the Elements, VII, Marcel Dekker Inc., New York, 1976, p. 293 (Chapter 2).
[30] P. Blanc, C. Madic, J.P. Launay, Inorg. Chem. 21 (1982) 2923.
[31] E. Gileadi, personal discussions.
[32] P. Chen, M.A. Fryling, R.L. McCreery, Anal. Chem. 67 (1995) 3115.
[33] R.L. McCreery, K.K. Cline, C.A. McDermott, M.T. McDermott, Colloids Surf. A 93 (1994) 211.
[34] C.A. McDermott, K.R. Kneten, R.L. McCreery, J. Electrochem. Soc. 140 (9) (1993) 2593.
[35] F.A. Cotton, G. Wilkinson, Advanced Inorganic Chemistry, fifth ed., John Wiley & Sons, New York, 1988, p. 665.
[36] C.F. Baes Jr., R.E. Mesmer, The Hydrolysis of Cations, John Wiley & Sons, New York, 1976, p. 197.
[37] R.R. Dogonadze, J. Ulstrup, Yu.I. Kharkats, J. Electroanal. Chem. 39 (1972) 47.
[38] R.R. Dogonadze, J. Ulstrup, Yu.I. Kharkats, J. Electroanal. Chem. 43 (1973) 161.
[39] W. Schmickler, J. Electroanal. Chem. 137 (1982) 189.